Electrochimica Acta 483 (2024) 144007

Contents lists available at ScienceDirect

Electrochimica Acta

journal homepage: www.journals.elsevier.com/electrochimica-acta

Poly(ethylene glycol)(PEG)-cryogels: A novel platform towards enzymatic electrochemiluminescence (ECL)-based sensor applications

Lucia Simona Ferraraccio [a,b], James Russell [c], Ben Newland [d], Paolo Bertoncello [a,b,*]

[a] Department of Chemical Engineering, Faculty of Science and Engineering, Swansea University Bay Campus, Crymlyn Burrows, Swansea SA1 8EN, United Kingdom
[b] Centre for NanoHealth, Swansea University, Singleton Campus, Swansea SA2 8PP, United Kingdom
[c] AIM Facility, Faculty of Science and Engineering, Swansea University Bay Campus, Crymlyn Burrows, Swansea SA1 8EN, United Kingdom
[d] School of Pharmacy and Pharmaceutical Sciences, Cardiff University, King Edward VII Avenue, Cardiff CF10 3NB, United Kingdom

ARTICLE INFO

Keywords:
Electrochemiluminescence
Electropolymerization
Enzyme
Encapsulation
PEG-cryogel

ABSTRACT

Enzymes-based electrochemical biosensors require the immobilisation of the enzymes on the electrode surfaces as well as their storage in aqueous environments to maintain the enzymatic activity. Herein, we described an enzyme-based electrochemiluminescence biosensor fabricated by incorporating oxidase enzymes (horseradish peroxidase, HRP; glucose, GOx, lactate, LOx, and cholesterol oxidases, ChOx) within poly(ethylene glycol)diacrylate (PEGDA) cryogels, which retain their activity when stored in dry conditions. The redox reactions between the oxidase enzymes and their corresponding substrates produce hydrogen peroxide that can be detected in the presence of a layer of polyluminol deposited on the electrode surface. These oxidases PEG-based cryogels were characterized using cyclic voltammetry and electrochemiluminescence (ECL) to assess the redox reactions between the enzymes and the corresponding substrates. The proposed biosensors were characterised by good stability and repeatability with a calculated limit of detections (LODs) in the micromolar concentration range. The performances of PEG cryogels over the time evidenced the stability of the as-prepared materials up to 30 days in dry conditions, confirming good retention of the encapsulated enzymes. Furthermore, the biosensors were tested in the presence of interferent species showing good selectivity. Finally, these oxidases-PEG cryogels were tested in real samples (commercial contact lenses, artificial sweat and commercial milk) confirming the suitability of such material for the detection of hydrogen peroxide with calculated LoDs as 10.37 ± 0.4 μM for HRP/contact lenses liquid; 3.87 ± 0.3 μM for GOx/artificial sweat; 1.09 ± 0.6 μM for LOx/artificial sweat; and 6.59 ± 0.5 for ChOx/milk.

1. Introduction

Since the first example of enzyme-based electrochemical biosensor developed by Clark and Lyons in 1962 [1] with glucose oxidase as a recognition element for the detection of glucose, the use of enzymes has seen considerable technological advancements. Such enzymatic electrochemical biosensors allow fast analysis of important parameters applicable is several fields such as clinical diagnosis [2–4], environmental monitoring [5,6], food industry [7,8] and water treatment [9,10].

Enzymatic electrochemical biosensors are characterized by the great advantage of high specificity towards the substrate, fast response time, and ability to operate using small amount of volumes [11]. Typically, enzymes show optimum activity when they are in solution, however, for practical electroanalytical applications, the immobilization of the enzyme on the electrode surface is required, as it allows the use of minimum amounts of expensive enzymes. However, the immobilisation of the enzyme on the electrode surface is associated with steric hindrance that limits the activity of the enzyme by preventing the access of the substrate to the active sites of the enzyme.

Over the years several immobilization strategies have been developed. In general, four methods of immobilization have been developed during the years: (i) adsorption; (ii) covalent bonding, (iii) bioconjugation, and (iv) physical entrapment [12]. Adsorption and deposition are non-covalent strategies which involve the use of electrostatic interactions with the electrode surfaces [13]. The covalent methods

* Corresponding author at: Department of Chemical Engineering, Faculty of Science and Engineering, Swansea University Bay Campus, Crymlyn Burrows, Swansea SA1 8EN, United Kingdom.
E-mail address: p.bertoncello@swansea.ac.uk (P. Bertoncello).

https://doi.org/10.1016/j.electacta.2024.144007
Received 26 October 2023; Received in revised form 13 February 2024; Accepted 25 February 2024
Available online 28 February 2024

instead, allow a more stable attachment of the protein to the electrode forming a covalent bond [14]. For example, one of the most popular covalent methods is the cross-linking of glutaraldehyde with arrays containing amino groups to immobilize enzymes on electrode surfaces. The bio-conjugation approach consists in the formation of an interface between a biomolecule and another molecule or material characterised by a covalent bond [15]. Finally, the physical entrapment is one of the most used immobilization methods, as it avoids the modification of the structure of the enzymes which are very fragile. This technique is applicable for most of enzymes, and antibodies and it is widely used for the development of biosensors as the matrices used for the encapsulation protect the enzymes from the external environmental changes such as pH and temperature [16,17].

All these strategies aimed at maximising the anchoring of the enzymes on various electrode surfaces such as screen-printed electrodes [18], glassy carbon electrodes [19], carbon nanotube electrodes [20,21] that require the storage of the enzyme-functionalised electrode in buffer solutions to preserve the enzymatic activity. The properties of the matrix used for the immobilisation process are crucial for the determination of the enzyme performance. The matrix needs to be inert toward the hosted enzyme, biocompatible, resistant to the external environment (especially temperature and pH changes), hydrophilic, and porous to allow the diffusion of the substrate and ions [22].

Hydrogels have been widely used as an immobilisation matrix due to their hydrophilicity and biocompatibility [16,23–26]. However, these hydrogels are problematic in terms of storage and ease-of-use, as they require to remain hydrated to work. Recently, macroporous hydrogels obtained at sub-zero degrees Celsius temperatures, also known as cryogels, have received special attention in tissue engineering applications due to their highly macroporous interconnected structure and ability to be dried, sterilised and stored prior to re-hydration and use [27–29]. Cryogels are used in bio-scaffolding as their porous three-dimensional structure allows easy cellular ingrowth and free diffusion of solutes [30–32]. The use of cryogels as a matrix for enzyme immobilization are widely reported in literature. Examples include poly(vinyl alcohol) (PVA)-cryogels [14,33], albumin-chitosan cryogel [34], poly (2-hydroxyethyl methacrylate) p(HEMA)-cryogels [35], oligoethylene glycol (OEG)-cryogels [36], apatite (ACGs)-cryogels [37], glycosaminoglycans (GAGs) cryogels [38], synthetic poly(ethylene glycol) (PEG) in combination with other materials such as collagen, agarose and heparin [39–42] but also stand-alone [43,44]. Nonetheless, none of these materials have been used so far to develop ECL-based biosensors. ECL is an analytical method that is attracting strong interest in electroanalysis in virtue of its high sensitivity, reproducibility, and simplicity of the apparatus [45–49].

In this work, we report the first example of ECL biosensor based on poly (ethylene glycol) (PEG)-based-cryogels with incorporated oxidase enzymes (glucose oxidase, lactate oxidase, horseradish peroxidase and cholesterol oxidase) and using electropolymerized luminol (polyluminol) as the luminophore probe. Both the oxidases-PEG-based-cryogels and the luminophore are confined on the electrode surface. Also, we have estimated the activity of the oxidases enzymes by measuring the ECL emission from polyluminol in the presence of the hydrogen peroxide produced during the redox reaction between the immobilized enzyme and the corresponding substrate. Interestingly, the enzymes encapsulated within the cryogels were characterised by high stability (up to months) and, crucially, can be stored in dry conditions and at room temperature still preserving the enzymatic activity.

2. Materials and methods

2.1. Materials

Poly(ethylene glycol) diacrylate (PEGDA, M_n=700 g/mol) and 2-hydroxy-2-methylpropiophenone (HMPP) for the synthesis of the cryogels, phosphate-buffered saline (PBS), sodium chloride (NaCl, ≥99 %), potassium chloride (KCl, 99 %), potassium hydroxide (KOH, ≥85 %), luminol (97 %), sodium hydroxide (NaOH, ≥98 %), D-(+)-glucose (≥99.5 %), cholesterol (≥99 %), L-lactic acid, horseradish peroxide (HRP), glucose oxidase (GOx), lactate oxidase (LOx), and cholesterol oxidase (ChOx), bovine serum albumin (BSA) conjugated Rhodamine were purchased from Merck; Triton X-100, and ethanol (EtOH, 99 %) were purchased from Fisher Scientific; hydrogen peroxide (H_2O_2, 35 %) was purchased from SAFC. All the solutions were prepared using MilliQ water with resistivity at 18 MΩ cm at 25 °C. Polystyrene templates for cryogel synthesis were produced with the dimensions of 0.5 mm thickness and 1 mm diameter as previously described [50].

2.2. Synthesis of PEG-based cryogels and encapsulation of enzymes procedure

The enzymes were encapsulated within the cryogels using photochemical crosslinking in polystyrene templates with one side covered by Scotch Magic™ Tape (Maplewood, Minnesota, USA). The PEGDA aqueous precursor solution was prepared by mixing 70 mg/mL of PEGDA monomer and 1 % (wt/vol) of the photoinitiator HMPP. The enzyme stock solutions (0.1875 mg/mL) were added to the PEGDA solution obtaining a final volume of 4 μL. 0.25 μL of the solution were added to each cavity of the template and then placed in the freezer at -20 °C for 20 min. Then, the templates were exposed to the UV light (365 nm wavelength) for 1 min whilst still in the freezer at -20 °C and 1 min outside the freezer at the same wavelength. After the photochemical crosslinking the tape was removed from the polystyrene template and then the cryogels were removed from the cavity with a pipette tip, then washed twice with ethanol and MilliQ water. Finally, the cryogels were dried at the temperature of 27 °C for 30 min.

2.3. SEM and confocal microscopy analysis of cryogels

SEM images were recorded using a Zeiss Evo LS25 SEM (Zeiss, Cambridge, UK) utilising the controlled pressure mode set to a target value of 30 Pa. This allowed for the non-conductive cryogels to be imaged without the need for coating. Confocal microscope images were taken using the SP5 confocal microscope (Leica) using the 10x lens, with a projected average image over a 40 μm z-length with a 5 μm gap between images. Cryogels were synthesised as described above, but with the addition of iFluor 647 maleimide (Stratech Ltd) at 0.001% wt/volume in the precursor solution. This wavelength is not photo-bleached by the UV initiated crosslinking. Bovine serum albumin (BSA) conjugated Rhodamine was used a fluorescent model of the enzyme encapsulation and encapsulated using the above protocol at the same concentrations as the enzymes.

2.4. Electrochemical and ECL characterisation of cryogel-modified GCE

Prior to the electrode modification, GCEs were cleaned by mechanical polishing of the surface with different grades of alumina powders (0.1 and 0.05 μm), sonication in MilliQ water for 5 min and finally dried with compressed air to remove any residues. The electropolymerization of luminol was carried out using the procedure developed by Sassolas et al. with some modifications [51]. Briefly, the electrochemical polymerization of luminol was performed using a CH Instrument potentiostat model 705E. A three-electrode configuration electrochemical cell with a Ag/AgCl reference electrode, a Pt wire as counter electrode, and a 3 mm glassy carbon electrode as working electrode all purchased from IJ Cambria (UK). Differently from the reported method of Sassolas' group, the electrolytic solution was composed of 0.1 M NaH_2PO_4 and 0.1 M KCl, pH 8.0 with the addition of 1 mM of luminol from the stock solution of 50 mM luminol/1 mM KOH. The electropolymerization was performed in the potential range 0-1 V vs. Ag/AgCl using a scan rate of 0.05 Vs^{-1} and operating multiple cycles of cyclic voltammetry. For the ECL tests, a cholesterol bulk solution was prepared dissolving 0.2 g of cholesterol in

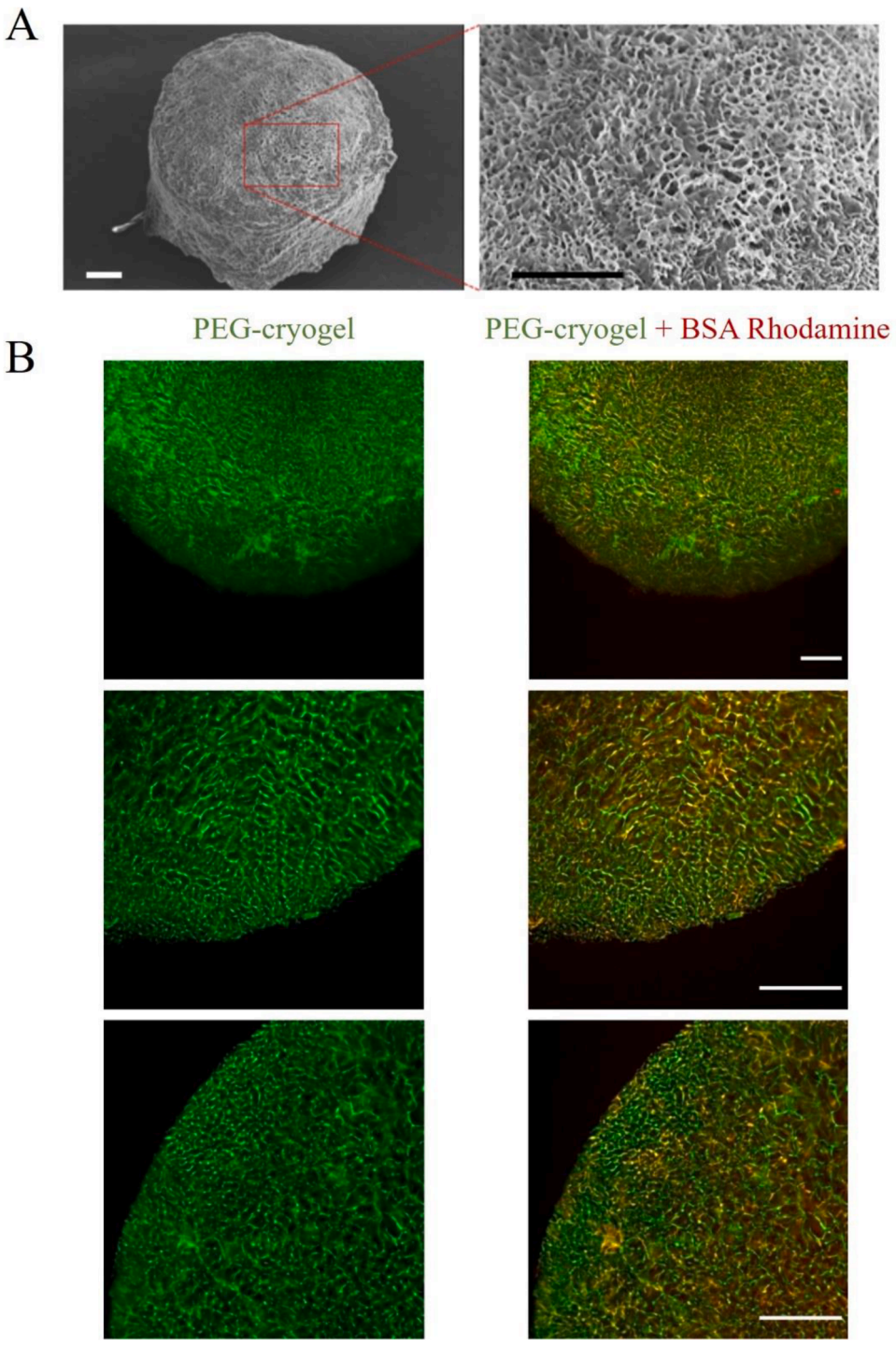

Fig. 1. The PEG based-cryogels exhibit a macroporous structure. (A) SEM images of the cryogel disc in the dehydrated state showing the pore and strut morphology. Scale bars = 100 μm. (B) Confocal laser scanning fluorescence microscopy (CLSM) images showing the PEG-based cryogels visualised via the incorporation of iFluor within the polymer structure (left) and after the addition of rhodamine-labelled bovine serum albumin (BSA)(right). Scale bars represent 100 μm.

5 mL of Triton-X-100 and 5 mL of isopropanol by heating at 50 °C. The solution was then diluted in 0.01 M PBS at pH 7.4 obtaining a 2 mM stock solution which was stored in the fridge at 4 °C. The analysis of the GOx and LOx-cryogels biosensors in real samples was performed using an artificial sweat solution obtained by mixing 300 mM NaCl, 40 mM urea, 100 mM L-lactic acid, 100 mM D-(+) glucose, in 100 mL distilled water. The stock solution was diluted in 0.01 M PBS and adjusted at pH 7.4 and stored at 4 °C. The HRP-cryogel was tested with a commercial contact lenses solution and dilute in 0.01 M PBS obtaining a stock solution of 20 mM concentrations and stored at 4 °C. Finally, the ChOx-cryogel was tested in commercial milk and diluted in 0.01 M PBS at pH 7.4 obtaining a 1 mM stock solution stored at 4 °C.

3. Results and discussion

3.1. Microscopic characterization

Scanning electron microscopy (SEM) (Fig. 1A) images show the

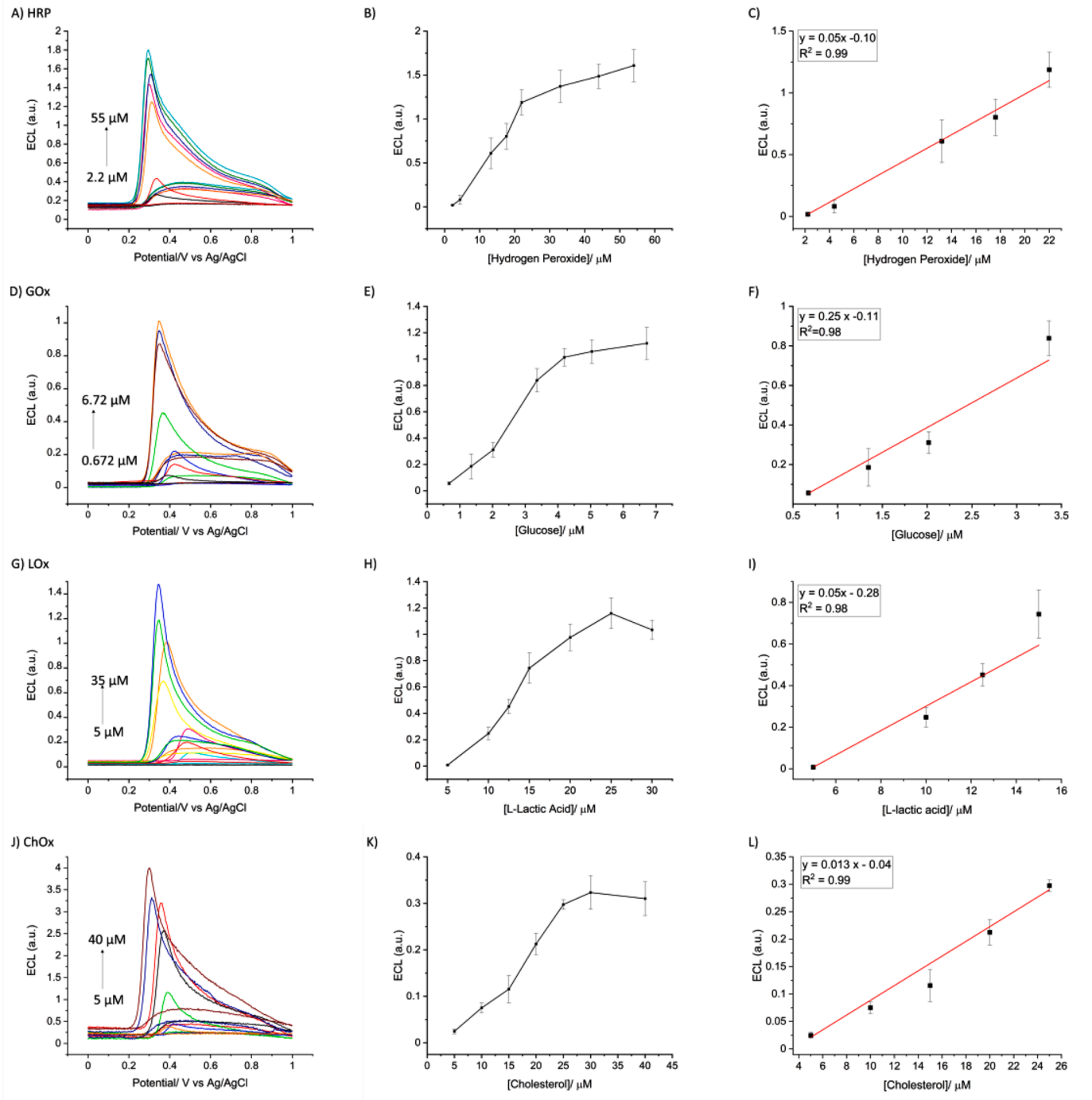

Fig. 2. ECL response of PEG-cryogels loaded with oxidases on polyluminol-modified GCE. (A) HRP-cryogel and (B) calibration curve of ECL response vs. concentration of hydrogen peroxide; (D) GOx- cryogel and (E) calibration curve vs. concentration of glucose; (G) LOx- cryogel and (H) calibration curve vs. concentration of L-lactic; (J) ChOx-cryogel and (K) calibration curve vs. concentration of cholesterol. The ECL experiments were performed at scan rate of 0.05 V s^{-1} in 0.01 M PBS supporting electrolytes for all enzymes, pH 9.0 (HRP, GOx, ChOx), and pH 7.4 (LOx). Inset plots (C, F, I, and L) represent the linear range. The error bars represent the standard deviation from three repetitions.

macroporous structure of the dehydrated materials, which is typical of cryogelated biomaterials. This pore structure was further visualised in the hydrated state via confocal laser scanning fluorescence microscopy (CLSM) (Fig. 1B).

Fig. 1B evidence the porous structure of PEG-cryogels. These pores look highly interconnected and in agreement with literature [52]. This porosity confirms an efficient flow of the luminophore into the PEG matrix, which suggests ease of diffusion also for the substrates for the redox reactions to occur.

3.2. Electrochemical and ECL characterisation of cryogels

An important aspect in the development of ECL-based biosensors is the immobilization of the luminophore on the electrode surface. The presence of the luminophore in the solid state rather than in solution is very advantageous as the use of the expensive luminophore is minimized and allows the possibility of reusing the same electrode multiple times. A typical example is the immobilisation of tris(2,2′ -bipyridyl)ruthenium (II) in polymer matrices [53]. Here, we deposited a polyluminol film on

Table 1
Comparison of the PEG-Cryogel/Polyluminol biosensors performances with others in literature.

Enzyme	Encapsulation	Detection technique	LOD molarity	Linear range molarity	Refs.
HRP	HRP/PGN/GCE	Amperometric	0.0267 nM	0.08 nM–835 μM	[62]
HRP	HRP/peptide	EIS, CV, CA	0.03 μM	0.1 μM - 0.1 mM	[63]
HRP	HRP/$Cu_3(PO_4)_2$	UV–VIS	–	100 nM - 100 μM	[64]
HRP	NH_2-CDs	CV	1.8 nM	5 μM - 590 nM	[65]
HRP	Absorption	Hydrodynamic voltammetry	0.2 μM	20 μM -2.5 mM	[66]
HRP	Sol-gel	CL	0.67 μM	0.1 μM −3.0 mM	[67]
HRP	HRP-dsDNA/GO-QDs/GCE	ECL	0.5 pM	1.0 pM -0.1 μM	[68]
HRP	Alginate hydrogel	ECL	5.38 ± 0.05 μM	4.4 μM - 22 μM	[26]
HRP	**PEG-cryogel**	**ECL**	**1.9 μM**	**2.2 μM -22 μM**	**This work**
GOx	Absorption	Hydrodynamic voltammetry	20 μM	20 μM -160 μM	[66]
GOx	polyNiTSPc/MWNTs	ECL	0.08 μM	1.0 μM -1 mM	[69]
GOx	PtNFs/GO/GODx	ECL	2.8 μM	5 μM -80 μM	[70]
GOx	Covalent binding	ECL	0.3 mM	0–10 mM	[71]
GOx	Cu-MOFs/GOx	BP-ECL	0.05 pM	0.1 pM -0.1 μM	[72]
GOx	Entrapment in NanoPANi	CV	0.3 ± 0.1 μM	0.01 μM -5.5 mM	[73]
GOx	GOx–graphene/GC	Voltammetry	10±2 μM	0.1 μM -10 mM	[74]
GOx	Alginate hydrogel	ECL	0.84 μM	0.56 μM -4.2 μM	[19]
GOx	**PEG-Cryogel**	**ECL**	**0.58 μM**	**0.672 μM – 4.2 μM**	**This work**
LOx	Immobilised in Nafion	Amperometric	1 μM	Up to 0.8 mM	[75]
LOx	LOx/PB-modified SPE	Amperometric	0.005 mM	0.005 μM - 5.000 mM	[76]
LOx	MN-PEGDA/LOx	CV	1 μM	0–4 mM	[77]
LOx	Immobilised eggshell	Amperometric	8.6 μM	0.00–0.48 mM	[78]
LOx	MWCNT-polypyrrole/LOx	Chronoamperometry	51 μM	1 μM −15 mM	[79]
LOx	$H_2Ti_3O_7$/TNT/LOx	CV,amperometry	0.2 mM	0.5 μM −14 mM	[80]
LOx	Alginate hydrogel	ECL	0.50±0.03 μM	2.6 μM −9.7 μM	[26]
LOx	**PEG-Cryogel**	**ECL**	**3.51 μM**	**5 μM −15 μM**	**This work**
ChOx	Chit/ChOx/$Ti_3C_2T_x$	SEM, CV, EIS, DPV	0.11 nM	0.3 μM - 4.5 nM	[81]
ChOx	Free	Direct amperometry	1 nM	1 μM – 7 mM	[82]
ChOx	Agarose hydrogel	Calorimetric	3.5 μM	10 μM – 100 μM	[83]
ChOx	Fused-silica capillary	Amperometric	12.4 μM	50 μM −1.0 mM	[84]
ChOx	Adsorption	Optical, gravimetric, CV	–	0–1 mM	[85]
ChOx	AuNPs/ChOx	CV, EIS	34.6 μM	0.04 μM - 0.22 mM	[86]
ChOx	CdSeTe/ZnS QDs-chitosan-ChOx	ECL	–	1.5 μM - 4.5 mM	[56]
ChOx	Free	Calorimetric	8.36 μM	50 μM – 6 mM	[87]
ChOx	**PEG-Cryogel**	**ECL**	**4.65 μM**	**5 μM −25 μM**	**This work**

the GCE using the method developed by Sassolas et al. with some important modifications [51,54,55]. For instance, the electropolymerization was carried out at much more alkaline values of pH (pH 8 here vs. pH 6 reported in the Sassolas' method) which allowed to maximize the ECL emission of polyluminol, which is well established to occur at high value of pH (from pH 8 and above). Three peaks were observed during the polymerization of luminol: peak I registered at ~0.3 V representing the luminol monomer oxidation which decreases during the polymerisation process as the monomer is consumed; peak II and peak III observed at ~ 0.55 V and ~ 0.25 V represent the oxidized and reduced forms of polyluminol, respectively (See S1). The observed peaks agree well with work from Sassolas et al. [54]. The results reported in the Supporting Information S1–S3 allowed us to optimize the conditions for the polyluminol formation on GCE. We found that 20 cycles lead to the formation of a polyluminol layer with the highest ECL signal (see S1, Table 1). Also, despite the optimum pH were found to be pH 9, we selected pH 8 as the working pH for the polymerization. In fact, the ECL signal at this pH provides a more stable value (lower error bars on repetitions), see S2. Finally, the optimum concentration of luminol for the polymerization of luminol was found to be 1 mM (see S3). To assess the electroactivity of the as prepared polyluminol film towards hydrogen peroxide detection, CVs and ECL of empty PEG-cryogels deposited onto these polyluminol films were recorded. This study was performed in 0.01 M PBS at pH 8.0 and scan rate 0.05 Vs^{-1} with the addition of different concentrations of hydrogen peroxide (see Fig. S4). The results highlighted that both the anodic peak currents (measured using CV) and light emission (measured using ECL) increase with the concentration of hydrogen peroxide indicating the electroactivity of the polyluminol film and that the deposition of cryogels onto the polyluminol-modified GCEs do not hinder the diffusion of hydrogen peroxide to the electrode surface. This is not surprising considering the porous structure of the cryogels. In addition, a study to select the optimum working pH for each enzyme (HRP, GOx, LOx, and ChOx) on the polyluminol-modified GCE was performed. Fig. S5 illustrate the related ECL response obtained with the four oxidases. As expected, the ECL signal is strongly dependent on the pH. The highest ECL signal for HRP, GOx and ChOx is obtained at pH 9, whereas for the LOx the highest ECL signal is recorded at pH 7.4, which is in agreement with data reported in literature [16]. Based on these results, we selected pH 9 for HRP, GOx and ChOx, and pH 7.4 for LOx in all subsequent experiments.

Furthermore, to ascertain whether the oxidases encapsulated within cryogels are suitable as an enzymatic biosensor platform, we deposited the oxidase-loaded cryogels on polyluminol-modified GCEs using the conditions selected from the preliminary experiments. The choice of such enzymes is due to the fact that these oxidases catalyse the reaction of hydrogen peroxide to water and oxygen (HRP) or produce hydrogen peroxide as a by-product of the enzymatic reactions with their corresponding substrate (GOx, LOx, and ChOx) [56–58]. The ECL analysis was performed in 0.01 M PBS by adjusting the pH with 0.1 M NaOH according to the optimum pH of each enzyme (see Fig. 2) in the presence of different concentrations of the substrates, e.g. hydrogen peroxide (A), glucose (D), L-lactic acid (G), and cholesterol (J). The calibration curves reported in Fig. 2 (B, E, H, and K) depict the ECL response obtained vs. the concentration of the various substrates. These results evidence good sensitivity of the ECL sensor for low concentrations of substrates added to the solution with sensitivity values of 0.46 μA mM^{-1} cm^{-2} for HRP-hydrogen peroxide, 3.11 μA mM^{-1} cm^{-2} for the GOx-glucose, 0.83 μA $mM^{-1}cm^{-2}$ for LOx-L-lactic acid, and 0.19 μA mM^{-1} cm^{-2} for the ChOx-cholesterol systems. The sensitivity values were calculated as the slope of the calibration curve for different concentrations of analytes added to the electrolytic solution [59]. The inset plots reported of Fig. 2, describe the linear range of each system and the corresponding correlation coefficient showing a linear dependence of the ECL signal with respect of the substrate concentrations.

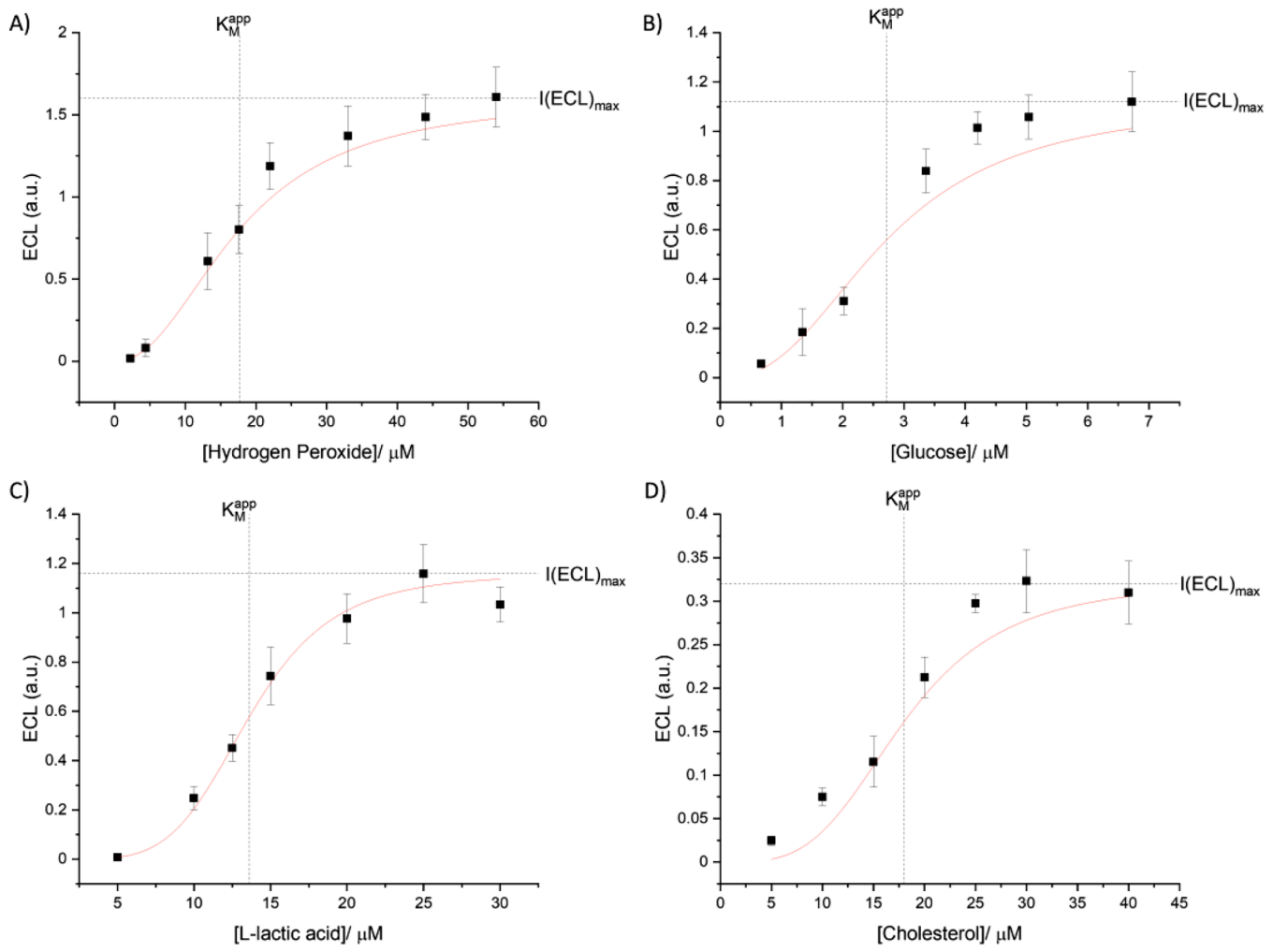

Fig. 3. Michaelis-Menten fitting and evaluation of the kinetics parameters. ECL vs. substrate concentration of (A) HRP-cryogel at pH 9.0, (B) GOx-cryogel at pH 9.0, (C) LOx-cryogel at pH 7.4, and (D) ChOx-cryogel at pH 9.0 recorded on polyluminol modified GCE, 0.01 M PBS, scan rate 0.05 Vs^{-1}. Each plot represents the maximum ECL intensity $I(ECL)_{max}$ achievable for each system and the apparent Michaelis-Menten constant obtained at the 50 % of the $I(ECL)_{max}$. Error bars represent the standard deviation from a triplicate data point.

We performed additional experiments using the same aforementioned conditions, however, rather than polyluminol we used luminol in solutions. The results reported in Fig. S6 show higher ECL response for the luminol in solution. This result is expected as the concentration of the luminophore on the electrode surface is higher when the luminol is in solution rather than in the polyluminol film. Nonetheless, the ECL responses recorded with the polyluminol depict the same trend as those recorded with luminol in solution. Table 2 reported in the Supporting Information section (see S6) reports the ECL values, the linear range, limit of detection, limit of quantification, and the correlation coefficients obtained for the various oxidases encapsulated within the cryogels. These values were compared with the analogous systems analysed using luminol in solution. The limit of detection was obtained by applying the $3\sigma_b/slope$ formula where σ_b represents the standard deviation of the intercept and indicates the lowest concentration at which the substrate can be detected [60]. The limit of quantification instead was calculated with the $10\sigma_b/slope$ criteria [61]. These results show that the ECL detection enables the quantification of low concentrations of hydrogen peroxide with high sensitivity. The calculated LoDs, LOQs and linear range values are all within the micromolar range and comparable with other system reported in literature (see Table 1 below). Note that the concentrations of the substrates (hydrogen peroxide, glucose, L-lactic acid, and cholesterol) are expected to be in the micromolar range in the real samples herein considered such as contact lenses solutions and milk.

3.3. Kinetic study of oxidase-cryogels deposited on polyluminol-modified GCE

The estimation of the enzymatic activity within the cryogel deposited on polyluminol-modified GCE was carried out using the Michaelis-Menten method by studying the reaction rate vs. the substrate of the enzyme analysed. As previously reported [16,88], the enzymatic activity is analysed through the oxidation peak of the CV and the ECL emission at increased concentrations of substrate. Fig. 3 depict the ECL plots vs. the substrate concentrations of the various oxidase-PEG-cryogels, underlying the values of $I(ECL)_{max}$ and the K_M^{app} which correspond to 50 % of the maximum obtainable ECL intensity.

Table 3 (see S7) summarizes the values of K_M^{app} and $I(ECL)_{max}$ obtained for the four oxidases demonstrating both the ability of the substrate to diffuse through the pores of the material as well as good retention of the enzymes within the cryogel matrix. A comparison is also shown with the ECL values obtained with the luminol in solution on the same table (see S7). The kinetic evaluation of the oxidase enzymes entrapped in the cryogels offers a prediction of the catalytic activity correlated with the emission of light that, in turn, is dependent from the substrate concentration. The parameters reported in Table 3, S7 demonstrate high affinity of the enzyme for the corresponding substrate, therefore the retention of the enzyme within the cryogels matrix. Furthermore, the structure, selectivity and catalytic properties of the

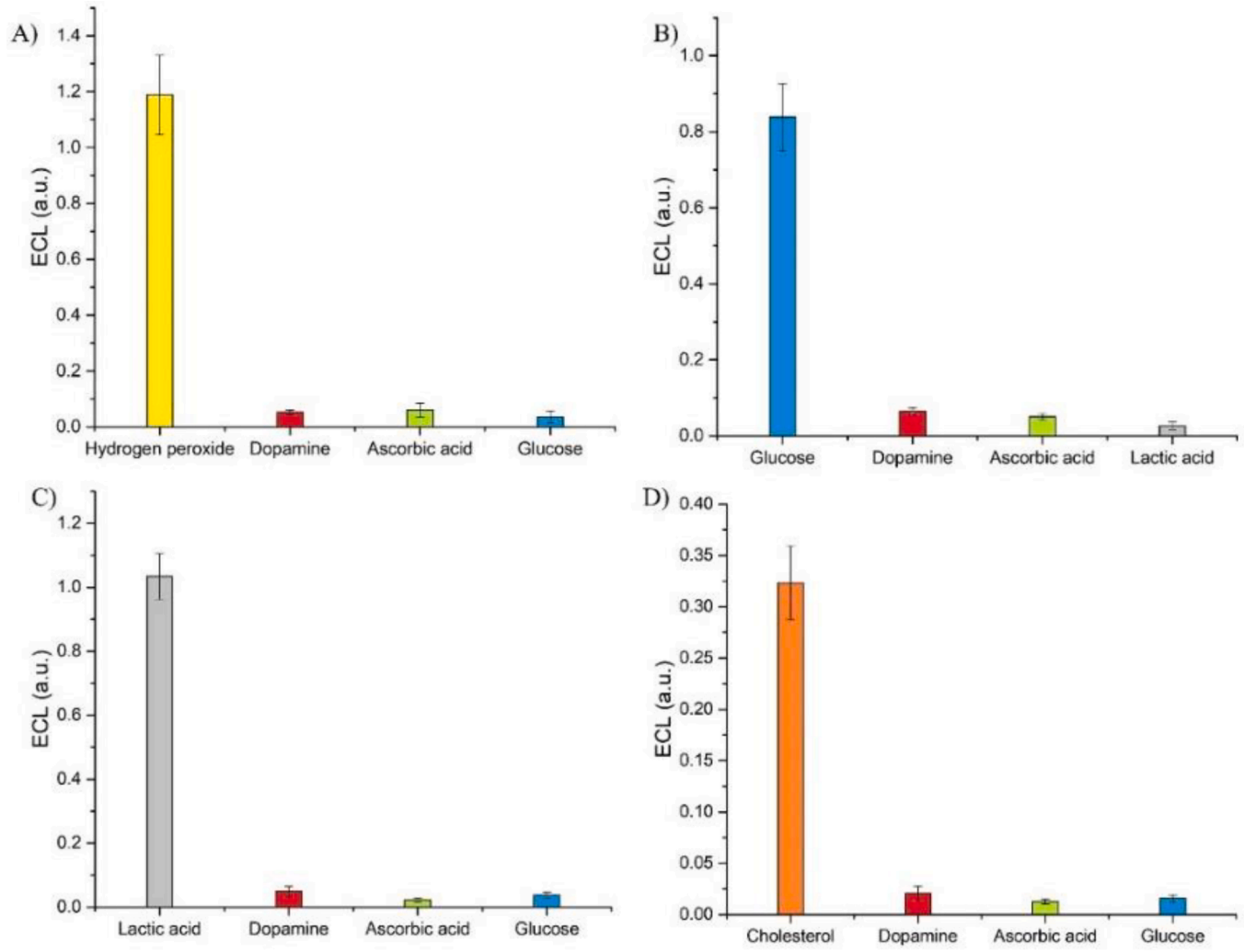

Fig. 4. Effect of the interferent species on the ECL response. (A) HRP-cryogel with 22 μM of H_2O_2, (B) GOx-cryogel with 3.36 μM of glucose, (C) LOx-cryogel with 20 μM of L-lactic acid, and (D) ChOx-cryogel with 25 μM of cholesterol. The experiments were recorded in 0.01 M PBS and scan rate 0.05 Vs^{-1} in the presence of 0.1 mM dopamine, 0.1 mM ascorbic acid, 0.1 mM glucose, and 0.1 mM lactic acid. The pH was adjusted to pH 9 for HRP, GOx, and ChOX, and pH 7.4 for LOx. Error bars represent the standard deviation from a triplicate data point.

oxidases is preserved. From the Michaelis-Menten equation, lower values of K_M^{app} correspond to high affinity of the enzyme towards the substrate. As formerly, we compared these values with those obtained with luminol in solution. The best values, as expected, were obtained with luminol in solution, however, it is remarkable that the values of K_M^{app} obtained with polyluminol e.g. 17.71 ± 0.37 for HRP, 2.72 ± 0.44 for GOx, 13.62 ± 0.54 for LOx, and 18.013 ± 0.68 for ChOx are very close to the corresponding values obtained with luminol (see Table 3, S7) as an indication of the preserved enzymatic activity. Note that the values obtained here with the oxidase-cryogels deposited on poly-luminol modified GCE are lower than the values obtained with other immobilization methods reported in literature, as an indication that the enzymes remain active within the PEG- cryogels [89]. Also noticeable, the K_M^{app} constants are slightly higher than the ones reported in our previous work with alginate hydrogels which were 7.71 ± 0.62 and 8.41 ± 0.43 μM for HRP and LOx, respectively [16]. This is expected, as the concentration of the luminophore (polyluminol), which is also consumed during the ECL reactions, is lower than the concentration of luminol in solution utilized in our previous work [16].

3.4. Interferences study of oxidase-cryogels

The selectivity of the oxidase encapsulated within the cryogels was investigated in the presence of common interferent species to determine the extent at which the ECL detection of hydrogen peroxide could be affected (see Fig. 4). ECL tests were performed in 0.01 M PBS at the corresponding optimum pH of each enzyme. The interferent species considered were ascorbic acid, dopamine, glucose, and L-lactic acid, each with a concentration of 0.1 mM, whereas the concentration of each enzyme substrate was 22 μM of H_2O_2, 3.36 μM of glucose (for the GOx interference study in Fig. 4B), 20 μM of L-lactic acid (Fig. 4C), and 25 μM of cholesterol (Fig. 4D). The results reported in Fig. 4 evidence that the oxidase encapsulated within the cryogels were not affected by the presence of these interferents, indicating both high selectivity and sensitivity towards low concentrations of the corresponding substrates.

3.5. Stability of the oxidase encapsulated within cryogels

A crucial aspect for the development of a biosensor is the preservation of the enzymatic stability, which in turn effects their efficiency and overall performances. Cryogels, contrary to the conventional hydrogels, can be stored in dry conditions, so they do not need to be constantly hydrated to maintain their properties. Moreover, the stability of the

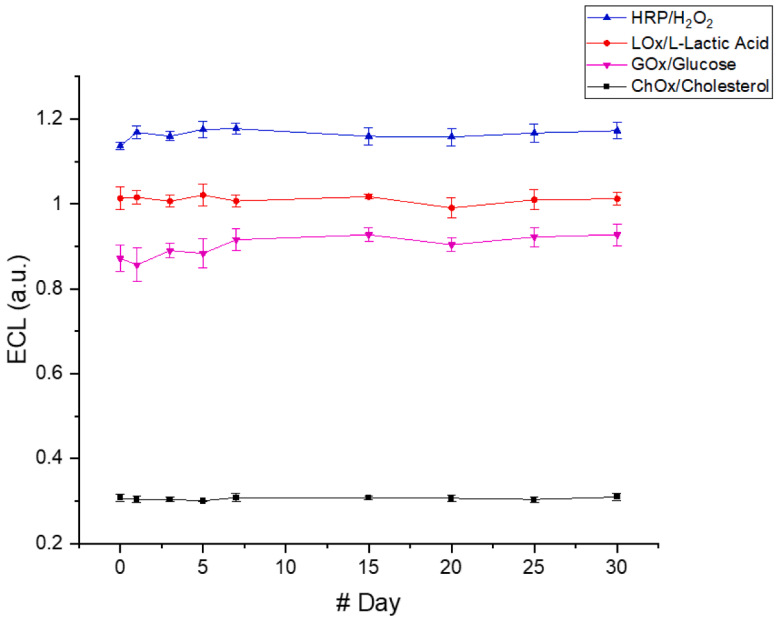

Fig. 5. Stability of oxidases encapsulated within PEG cryogel under dry conditions. ECL responses were recorded in 0.01 M PBS and scan rate of 0.05 Vs^{-1} over a period of 30 days. Calibration curve of HRP-cryogel in the presence of 22 μM concentration of hydrogen peroxide, and pH 9.0 (blue line). Calibration curve of GOx-cryogel in the presence of 3.36 μM concentration of glucose, and pH 9.0 (pink line). LOx-cryogel in the presence of 30 μM concentration of L-lactic acid and pH 7.4 (red line). Calibration curve of ChOx-cryogel in the presence of 30 μM cholesterol and pH 9.0 (black line). Error bars represent the standard deviation from a triplicate data point.

enzymes encapsulated within the cryogels was evaluated by studying the ECL signal over a 30-day time. The oxidases encapsulated within cryogels showed a remarkable stability when stored in dry conditions for 30 days before being hydrated and tested (see Fig. 5). This demonstrates the ability of such cryogels to preserve the catalytic activity of the enzyme over long time and up to several months. In contrast, the highly interconnected matrix of the cryogel recorded a loss of ca. 80 % of the enzyme activity when the cryogels were stored in aqueous solutions. As a model, we assessed the stability of HRP-cryogel with samples stored in 0.01 M PBS. The ECL signal measured in 15 days period drastically decreased after the first measurement (see Fig. S8).

3.6. *Validation of the ECL-biosensor: analysis of real samples*

The suitability of the sensors proposed here was finally tested for potential clinical investigations of important physiological parameters such as, glucose, lactic acid, and cholesterol. This validation is performed throughout the ECL response obtained in real samples from the production of hydrogen peroxide derived from the various enzymatic reactions of the four oxidases. For the HRP-cryogel, a commercial contact lenses solution was used, whereas for the GOx and LOx-cryogels, artificial sweat solution was prepared according to the work of Garcia-Rey et al. [16,90], and commercial milk for the ChOX- cryogel sensor. All real sample solutions were diluted in 0.01 M PBS to obtain a stock solution of 20 mM concentrations and added in different concentrations to the electrolytic solution. The ECL signals related to HRP (Fig. 6A), GOx (Fig. 6D), and LOx (Fig. 6G), and ChOx (Fig. 6J) evidence linear dependence with the corresponding concentration of the real sample. Noticeably, the HRP-cryogel presents a linear range between 15 and 45 μM of contact lenses solution with a correlation coefficient $R^2 = 0.99$ (Fig. 6C). As expected, the calibration curve (Fig. 6B) presents a dependence of the ECL from the different concentrations of contact lenses leading to a detection limit LoD = 10.37 ± 0.4 μM and LoQ = 31.4 ± 0.2 μM. For the GOx- cryogel the linear dependence of the ECL signal is over a range of 2.68–6.72 μM in artificial sweat solution added to 0.01 M PBS pH 9.0 (Fig. 6F). The calculated LoD is 3.87 ± 0.3 μM and LoQ as 11.74 ± 0.5 μM. (Fig. 6E). The LOx- cryogel was tested with different aliquots of sweat solution in 0.01 M PBS pH 7.4 finding a linear range in the range 2.2–20 μM (Fig. 6I), a correlation coefficient $R^2 = 0.99$, LoD = 1.09 ± 0.6 μM and LoQ = 71.7 ± 0.7 μM (Fig. 6H). Finally, the ChOx-cryogel was tested with different concentrations of commercial milk in 0.01 M PBS at pH 9.0 (Fig. 6J), giving a linear range of 10–30 μM with $R^2 = 0.99$ (Fig. 6L), LoD = 6.59 ± 0.5 μM and LoQ = 19.96 ± 0.3 μM (Fig. 6K).

The reproducibility and repeatability of the four oxidases-systems was tested in 0.01 M PBS (see S9) by studying the mean and standard deviation of six repetitions ($n = 6$) of six different modified GCEs. The results pointed out to a good reproducibility and repeatability highlighting further the suitability of the enzymes encapsulated within PEG-based cryogel platform for ECL-based sensing applications.

The accuracy of the ECL sensors was tested by studying the recovery of the substrates. The real samples solutions were spiked with known concentrations of the substrates and the% of recoveries reported in Table 2 highlights a high degree of accuracy of all the ECL analysed in this work.

4. Conclusions

In this work we proposed a novel biosensor based on the encapsulation of oxidases within cryogels synthesised from PEGDA to enhance their applicability over other systems such as hydrogels. These PEG cryogels were deposited onto polyluminol-modified glassy carbon electrodes for ECL analysis. We have demonstrated the versatility of the encapsulation of oxidase enzymes into PEG-based cryogels showing high selectivity and selectivity in the presence of interferent species and in the analysis of real samples. We showed that the use of PEG-cryogels as a matrix for the encapsulation is advantageous due to the high interconnected porous structure which allow the diffusion of the substrate for the redox reaction to the immobilized enzyme. For the first time, the oxidase enzymes were incorporated into cryogels and were tested using ECL detection of hydrogen peroxide. The results reported herein show high sensitivity and selectivity, with the calculated limit of detection for the four enzymes as LoD = 10.37 ± 0.4 μM for HRP system, LoD = 3.87 ± 0.3 μM for GOx, LoD = 1.09 ± 0.6 μM for LOx, and LoD = 6.59 ± 0.5

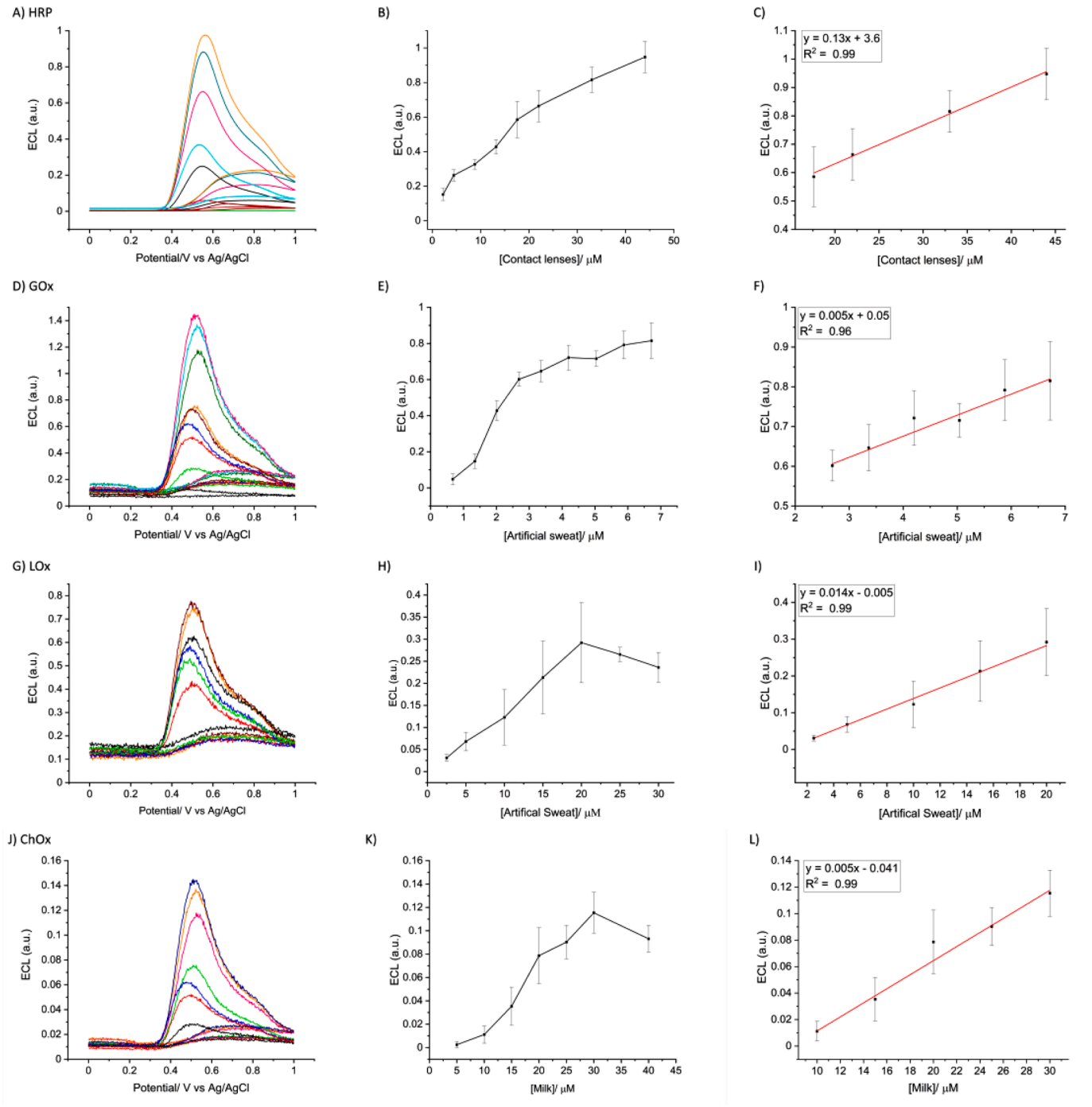

Fig. 6. Real sample analysis of oxidases encapsulated within the cryogels. HRP-cryogel vs. the concentration of contact lenses liquid in 0.01 M PBS pH 9.0 showing ECL(A) HRP), calibration curve and linear range (B,C); ECL (D) GOx), calibration curve and linear range (E, F) of GOx-cryogel in 0.01 M PBS at pH 9.0 with different concentrations of artificial sweat, ECL(G) LOx), calibration curve and linear range (H, I) of LOx-cryogel in 0.01 M PBS at pH 7.4, and ECL (J) ChOX), calibration curve (K) and linear range (L) of ChOX-cryogel in 0.01 M PBS at pH 9.0. The tests have been recorded at scan rate of 0.05 Vs^{-1}. Inset plots represent the linear range for the systems analysed containing the correlation coefficient R^2. Error bars represent the standard deviation from a data point of six repetitions.

Table 2
Concentrations and% of recoveries for hydrogen peroxide, glucose, L-lactic acid, and cholesterol from the ECL analysis of the corresponding spiked real samples.

Sample	Avg concn Calcd (μM)	% Recovery
H_2O_2 spiked contact lenses solution	19.02	98 %
Glucose spiked artificial sweat solution	2.37	99 %
L-lactic acid spiked artificial sweat solution	9.02	98 %
Cholesterol spiked milk solution	9.03	97 %

μM for ChOx. We highlight several advantages of the cryogel-based system over previously reported hydrogel systems. For example, they can be stored in dry conditions with a retention of the enzymatic activity up to 30 days (maximum time tested), and benefit from an easy and fast fabrication process. In conclusion, the oxidase PEG-based cryogels here proposed represent a promising platform for detection of physiological parameters such as glucose, L-lactic acid, and cholesterol with versatility for real-word use.

CRediT authorship contribution statement

Lucia Simona Ferraraccio: Data curation, Formal analysis, Investigation, Methodology, Validation, Visualization, Writing – original draft. **James Russell:** Investigation. **Ben Newland:** Investigation, Methodology, Resources, Writing – review & editing. **Paolo Bertoncello:** Conceptualization, Funding acquisition, Methodology, Project administration, Supervision, Writing – review & editing.

Declaration of competing interest

The authors declare that they have no competing financial interests or personal relationships that could have appeared to influence the work reported in this paper.

Data availability

Data will be made available on request.

Acknowledgments and Funding

L.S.F. gratefully acknowledges financial support from the Knowledge Economy Skills PhD Scholarship (KESS2) under the Welsh Government's European Social Fund (ESF) convergence program for West Wales and the Valleys and Perpetuus Carbon Ltd. P.B. acknowledges the Institute for Innovative Materials, Processing and Numerical Technologies (IMPACT) for the purchase of the ECL setup. The microscoscopic characterization was possible throughout the Advanced Imaging of Materials (AIM) facility (EPSRC Grant No. EP/M028267/1), the European Social Fund (ESF) through the European Union's Convergence programme administered by the Welsh Government (80708), and the Welsh Government Enhancing Competitiveness Grant (MA/KW/5554/19).

Supplementary materials

Supplementary material associated with this article can be found, in the online version, at doi:10.1016/j.electacta.2024.144007.

References

[1] L.C. Clark Jr, C. Lyons, Electrode systems for continuous monitoring in cardiovascular surgery, Ann. N. Y. Acad. Sci. 102 (1962) 29–45.
[2] R.S. Singh, T. Singh, A.K. Singh, Enzymes as diagnostic tools. Advances in Enzyme Technology, Elsevier, 2019, pp. 225–271.
[3] R. Monošík, M. Stred'anský, E. Šturdík, Application of electrochemical biosensors in clinical diagnosis, J. Clin. Lab. Anal. 26 (2012) 22–34.
[4] K. Mahato, S. Kumar, A. Srivastava, P.K. Maurya, R. Singh, P. Chandra, Electrochemical immunosensors: fundamentals and applications in clinical diagnostics. Handbook of Immunoassay Technologies, Elsevier, 2018, pp. 359–414.
[5] A. Amine, H. Mohammadi, I. Bourais, G. Palleschi, Enzyme inhibition-based biosensors for food safety and environmental monitoring, Biosens. Bioelectron. 21 (2006) 1405–1423.
[6] I. Karube, Y. Nomura, Enzyme sensors for environmental analysis, J. Mol. Catal. B Enzym. 10 (2000) 177–181.
[7] M.L. Verma, Enzymatic nanobiosensors in the agricultural and food industry, Nanosci. Food Agric. 4 (2017) 229–245.
[8] L.A. Terry, S.F. White, L.J. Tigwell, The application of biosensors to fresh produce and the wider food industry, J. Agric. Food Chem. 53 (2005) 1309–1316.
[9] S. Feng, H.H. Ngo, W. Guo, S.W. Chang, D.D. Nguyen, D. Cheng, S. Varjani, Z. Lei, Y. Liu, Roles and applications of enzymes for resistant pollutants removal in wastewater treatment, Bioresour. Technol. 335 (2021) 125278.
[10] J. Zdarta, K. Jankowska, K. Bachosz, O. Degórska, K. Kaźmierczak, L.N. Nguyen, L. D. Nghiem, T. Jesionowski, Enhanced wastewater treatment by immobilized enzymes, Curr. Pollut. Rep. 7 (2021) 167–179.
[11] H.H. Nguyen, S.H. Lee, U.J. Lee, C.D. Fermin, M. Kim, Immobilized enzymes in biosensor applications, Materials 12 (2019) 121.
[12] A.A. Homaei, R. Sariri, F. Vianello, R. Stevanato, Enzyme immobilization: an update, J. Chem. Biol. 6 (2013) 185–205.
[13] J. Deere, E. Magner, J.G. Wall, B.K. Hodnett, Mechanistic and structural features of protein adsorption onto mesoporous silicates, J. Phys. Chem. B 106 (2002) 7340–7347.
[14] M. Busto, V. Meza, N. Ortega, M. Perez-Mateos, Immobilization of naringinase from Aspergillus niger CECT 2088 in poly (vinyl alcohol) cryogels for the debittering of juices, Food Chem. 104 (2007) 1177–1182.
[15] C.S.M. Fernandes, G.D.G. Teixeira, O. Iranzo, A.C.A. Roque, Chapter 5 - Engineered protein variants for bioconjugation, B. Sarmento, J. das Neves (Eds.). Biomedical Applications of Functionalized Nanomaterials, Elsevier, 2018, pp. 105–138.
[16] L.S. Ferraraccio, D. Di Lisa, L. Pastorino, P. Bertoncello, Enzymes encapsulated within alginate hydrogels: bioelectrocatalysis and electrochemiluminescence applications, Anal. Chem. 94 (2022) 16122–16131.
[17] T.K. Hakala, T. Liitia, A. Suurnakki, Enzyme-aided alkaline extraction of oligosaccharides and polymeric xylan from hardwood kraft pulp, Carbohydr. Polym. 93 (2013) 102–108.
[18] G.S. Nunes, G. Jeanty, J.L. Marty, Enzyme immobilization procedures on screen-printed electrodes used for the detection of anticholinesterase pesticides: comparative study, Anal. Chim. Acta 523 (2004) 107–115.
[19] L.S. Ferraraccio, P. Bertoncello, Electrochemiluminescence (ECL) biosensor based on tris(2,2′-bipyridyl)ruthenium(II) with glucose and lactate dehydrogenases encapsulated within alginate hydrogels, Bioelectrochemistry. 150 (2023) 108365.
[20] C. Gutiérrez-Sánchez, W. Jia, Y. Beyl, M. Pita, W. Schuhmann, A.L. De Lacey, L. Stoica, Enhanced direct electron transfer between laccase and hierarchical carbon microfibers/carbon nanotubes composite electrodes. Comparison of three enzyme immobilization methods, Electrochim. Acta 82 (2012) 218–223.
[21] B. Dinesh, V. Mani, R. Saraswathi, S.M. Chen, Direct electrochemistry of cytochrome c immobilized on a graphene oxide–carbon nanotube composite for picomolar detection of hydrogen peroxide, RSC Adv. 4 (2014) 28229–28237.
[22] B.M. Brena, F. Batista-Viera, Immobilization of enzymes, J.M. Guisan (Ed.). Immobilization of Enzymes and Cells, Humana Press, Totowa, NJ, 2006, pp. 15–30.
[23] A.D. Augst, H.J. Kong, D.J. Mooney, Alginate hydrogels as biomaterials, Macromol. Biosci. 6 (2006) 623–633.
[24] S. Van Vlierberghe, P. Dubruel, E. Schacht, Biopolymer-based hydrogels as scaffolds for tissue engineering applications: a review, Biomacromolecules 12 (2011) 1387–1408.
[25] A. Herrmann, R. Haag, U. Schedler, Hydrogels and their role in biosensing applications, Adv. Healthc. Mater. 10 (2021) 2100062.
[26] L.S. Ferraraccio, D. Di Lisa, L. Pastorino, P. Bertoncello, Enzymes encapsulated within alginate hydrogels: bioelectrocatalysis and electrochemiluminescence applications, Anal. Chem. 94 (2022) 16122–16131.
[27] B. Newland, K.R. Long, Cryogel scaffolds: soft and easy to use tools for neural tissue culture, Neural Regen. Res. 17 (2022) 1981–1983.
[28] T.M. Henderson, K. Ladewig, D.N. Haylock, K.M. McLean, A.J. O'Connor, Cryogels for biomedical applications, J. Mater. Chem. B 1 (2013) 2682–2695.
[29] D. Eigel, R. Schuster, M.J. Männel, J. Thiele, M.J. Panasiuk, L.C. Andreae, C. Varricchio, A. Brancale, P.B. Welzel, W.B. Huttner, C. Werner, B. Newland, K. R. Long, Sulfonated cryogel scaffolds for focal delivery in *ex-vivo* brain tissue cultures, Biomaterials 271 (2021) 120712.
[30] B. Newland, F. Ehret, F. Hoppe, D. Eigel, D. Pette, H. Newland, P.B. Welzel, G. Kempermann, C. Werner, Macroporous heparin-based microcarriers allow long-term 3D culture and differentiation of neural precursor cells, Biomaterials 230 (2020) 119540.
[31] M. Jurga, M.B. Dainiak, A. Sarnowska, A. Jablonska, A. Tripathi, F.M. Plieva, I. N. Savina, L. Strojek, H. Jungvid, A. Kumar, B. Lukomska, K. Domanska-Janik, N. Forraz, C.P. McGuckin, The performance of laminin-containing cryogel scaffolds in neural tissue regeneration, Biomaterials 32 (2011) 3423–3434.
[32] D. Eigel, C. Werner, B. Newland, Cryogel biomaterials for neuroscience applications, Neurochem. Int. 147 (2021) 105012.
[33] S. Das-Bradoo, I. Svensson, J. Santos, F. Plieva, B. Mattiasson, R. Hatti-Kaul, Synthesis of alkylgalactosides using whole cells of Bacillus pseudofirmus species as catalysts, J. Biotechnol. 110 (2004) 273–286.
[34] M. Hedström, F. Plieva, I.Y. Galaev, B. Mattiasson, Monolithic macroporous albumin/chitosan cryogel structure: a new matrix for enzyme immobilization, Anal. Bioanal. Chem. 390 (2008) 907–912.
[35] S. Demirci, M. Sahiner, S. Yilmaz, E. Karadag, N. Sahiner, Enhanced enzymatic activity and stability by *in situ* entrapment of α-Glucosidase within super porous p (HEMA) cryogels during synthesis, Biotechnol. Rep. 28 (2020) e00534.
[36] X. Feng, J. Liu, G. Xu, X. Zhang, X. Su, W. Li, A. Zhang, Thermoresponsive double network cryogels from dendronized copolymers showing tunable encapsulation and release of proteins, J. Mater. Chem. B 6 (2018) 1903–1911.
[37] P.J. Jiang, G. Wynn-Jones, L.M. Grover, A calcium phosphate cryogel for alkaline phosphatase encapsulation, J. Mater. Sci. 45 (2010) 5257–5263.
[38] A. Wartenberg, J. Weisser, M. Schnabelrauch, Glycosaminoglycan-based cryogels as scaffolds for cell cultivation and tissue regeneration, Molecules 26 (2021) 5597.
[39] B. Newland, P.B. Welzel, H. Newland, C. Renneberg, P. Kolar, M. Tsurkan, A. Rosser, U. Freudenberg, C. Werner, Tackling cell transplantation anoïkis: an injectable, shape memory cryogel microcarrier platform material for stem cell and neuronal cell growth, Small 11 (2015) 5047–5053.
[40] Y. Hwang, C. Zhang, S. Varghese, Poly (ethylene glycol) cryogels as potential cell scaffolds: effect of polymerization conditions on cryogel microstructure and properties, J. Mater. Chem. 20 (2010) 345–351.
[41] T.D. Sargeant, A.P. Desai, S. Banerjee, A. Agawu, J.B. Stopek, An *in situ* forming collagen–PEG hydrogel for tissue regeneration, Acta Biomater. 8 (2012) 124–132.
[42] B.J. DeKosky, N.H. Dormer, G.C. Ingavle, C.H. Roatch, J. Lomakin, M.S. Detamore, S.H. Gehrke, Hierarchically designed agarose and poly (ethylene glycol) interpenetrating network hydrogels for cartilage tissue engineering, Tissue Eng. Part C Methods 16 (2010) 1533–1542.

[43] J. Wu, Q. Zhao, J. Sun, Q. Zhou, Preparation of poly (ethylene glycol) aligned porous cryogels using a unidirectional freezing technique, Soft Matter 8 (2012) 3620–3626.
[44] T. Dispinar, W. Van Camp, L.J. De Cock, B.G. De Geest, F.E. Du Prez, Redox-responsive degradable PEG cryogels as potential cell scaffolds in tissue engineering, Macromol. Biosci. 12 (2012) 383–394.
[45] R.J. Forster, P. Bertoncello, T.E. Keyes, Electrogenerated chemiluminescence, Annu. Rev. Anal. Chem. 2 (2009) 359–385.
[46] P. Bertoncello, P. Ugo, Recent advances in electrochemiluminescence with quantum dots and arrays of nanoelectrodes, ChemElectroChem. 4 (2017) 1663–1676.
[47] C. Meng, S. Knežević, F. Du, Y. Guan, F. Kanoufi, N. Sojic, G. Xu, Recent advances in electrochemiluminescence imaging analysis, eScience 2 (2022) 591–605.
[48] X. Ying, L. Zhou, W. Fu, Y. Wang, B. Su, Electrochemiluminescence devices for point-of-care testing, Sens. Diagn. 2 (2023) 480–491.
[49] A. Abdussalam, G. Xu, Recent advances in electrochemiluminescence luminophores, Anal. Bioanal. Chem. 414 (2022) 131–146.
[50] D. Eigel, L. Zoupi, S. Sekizar, P.B. Welzel, C. Werner, A. Williams, B. Newland, Cryogel scaffolds for regionally constrained delivery of lysophosphatidylcholine to central nervous system slice cultures: a model of focal demyelination for multiple sclerosis research, Acta Biomater. 97 (2019) 216–229.
[51] A. Sassolas, L.J. Blum, B.D. Leca-Bouvier, Electrogeneration of polyluminol and chemiluminescence for new disposable reagentless optical sensors, Anal. Bioanal. Chem. 390 (2008) 865–871.
[52] S.A. Bencherif, R.W. Sands, D. Bhatta, P. Arany, C.S. Verbeke, D.A. Edwards, D. J. Mooney, Injectable preformed scaffolds with shape-memory properties, Proc. Natl. Acad. Sci. U. S. A. 109 (2012) 19590–19595.
[53] P. Bertoncello, L. Dennany, R.J. Forster, P.R. Unwin, Nafion– Tris (2-2 '-bipyridyl) ruthenium (II) Ultrathin Langmuir– Schaefer films: redox catalysis and electrochemiluminescent properties, Anal. Chem. 79 (2007) 7549–7553.
[54] A. Sassolas, L.J. Blum, B.D. Leca-Bouvier, New electrochemiluminescent biosensors combining polyluminol and an enzymatic matrix, Anal. Bioanal. Chem. 394 (2009) 971–980.
[55] A. Sassolas, L.J. Blum, B.D. Leca-Bouvier, Polymeric luminol on pre-treated screen-printed electrodes for the design of performant reagentless (bio) sensors, Sens. Actuators B Chem. 139 (2009) 214–221.
[56] E.J.O.R. Alasdair J.Stewart, R. D.Moriarty, P. Bertoncello, T.E. Keyes, R.J. Forster, L. Dennany, A cholesterol biosensor based on the NIR electrogenerated-chemiluminescence (ECL) of water-soluble CdSeTe/ZnS quantum dots, Electrochim. Acta 157 (2015) 8–14.
[57] J.R. Anusha, C.J. Raj, B.B. Cho, A.T. Fleming, K.H. Yu, B.C. Kim, Amperometric glucose biosensor based on glucose oxidase immobilized over chitosan nanoparticles from gladius of Uroteuthis duvauceli, Sens. Actuators B Chem. 215 (2015) 536–543.
[58] D. Pfeiffer, B. Möller, N. Klimes, J. Szeponik, S. Fischer, Amperometric lactate oxidase catheter for real-time lactate monitoring based on thin film technology, Biosens. Bioelectron. 12 (1997) 539–550.
[59] A.A. Odeh, Y. Al-Douri, C.H. Voon, R. Mat Ayub, S.C.B. Gopinath, R.A. Odeh, M. Ameri, A. Bouhemadou, A needle-like Cu_2CdSnS_4 alloy nanostructure-based integrated electrochemical biosensor for detecting the DNA of Dengue serotype 2, Microchim. Acta 184 (2017) 2211–2218.
[60] J. Pum, Chapter Six - A practical guide to validation and verification of analytical methods in the clinical laboratory, G.S. Makowski (Ed.). Advances in Clinical Chemistry, Elsevier, 2019, pp. 215–281.
[61] P. Konieczka, 2.31 - Validation and regulatory issues for sample preparation, J. Pawliszyn (Ed.). Comprehensive Sampling and Sample Preparation, Academic Press, Oxford, 2012, pp. 699–711.
[62] Y. Liu, X. Liu, Z. Guo, Z. Hu, Z. Xue, X. Lu, Horseradish peroxidase supported on porous graphene as a novel sensing platform for detection of hydrogen peroxide in living cells sensitively, Biosens. Bioelectron. 87 (2017) 101–107.
[63] J. Zhao, Y. Yan, L. Zhu, X. Li, G. Li, An amperometric biosensor for the detection of hydrogen peroxide released from human breast cancer cells, Biosens. Bioelectron. 41 (2013) 815–819.
[64] C. Yang, M. Zhang, W. Wang, Y. Wang, J. Tang, UV–Vis detection of hydrogen peroxide using horseradish peroxidase/copper phosphate hybrid nanoflowers, Enzyme Microb. Technol. 140 (2020) 109620.
[65] Y. Su, X. Zhou, Y. Long, W. Li, Immobilization of horseradish peroxidase on amino-functionalized carbon dots for the sensitive detection of hydrogen peroxide, Microchim. Acta 185 (2018) 114.
[66] E. Csöregi, L. Gorton, G. Marko-Varga, Amperometric microbiosensors for detection of hydrogen peroxide and glucose based on peroxidase-modified carbon fibers, Electroanalysis 6 (1994) 925–933.
[67] A. Navas Díaz, M.C. Ramos Peinado, M.C. Torijas Minguez, Sol–gel horseradish peroxidase biosensor for hydrogen peroxide detection by chemiluminescence, Anal. Chim. Acta 363 (1998) 221–227.
[68] Z.J. He, T.F. Kang, L.P. Lu, S.Y. Cheng, An electrochemiluminescence aptamer sensor for chloramphenicol based on GO-QDs nanocomposites and enzyme-linked aptamers, J. Electroanal. Chem. 860 (2020) 113870.
[69] B. Qiu, Z. Lin, J. Wang, Z. Chen, J. Chen, G. Chen, An electrochemiluminescent biosensor for glucose based on the electrochemiluminescence of luminol on the nafion/glucose oxidase/poly(nickel(II)tetrasulfophthalocyanine)/multi-walled carbon nanotubes modified electrode, Talanta 78 (2009) 76–80.
[70] X. Tian, S. Lian, L. Zhao, X. Chen, Z. Huang, X. Chen, A novel electrochemiluminescence glucose biosensor based on platinum nanoflowers/graphene oxide/glucose oxidase modified glassy carbon electrode, J. Solid State Electrochem. 18 (2014) 2375–2382.
[71] J. Kremeskotter, R. Wilson, D. Schiffrin, B.J. Luff, J.S. Wilkinson, Detection of glucose via electrochemiluminescence in a thin-layer cell with a planar optical waveguide, Meas. Sci. Technol. 6 (1995) 1325.
[72] C. Chen, Y.L. Wang, X. Lin, S.H. Ma, J.T. Cao, Y.M. Liu, Cu-MOFs/GOx bifunctional probe-based synergistic signal amplification strategy: toward highly sensitive closed bipolar electrochemiluminescence immunoassay, ACS Appl. Mater. Interfaces 15 (2023) 22959–22966.
[73] Z. Wang, S. Liu, P. Wu, C. Cai, Detection of glucose based on direct electron transfer reaction of glucose oxidase immobilized on highly ordered polyaniline nanotubes, Anal. Chem. 81 (2009) 1638–1645.
[74] P. Wu, Q. Shao, Y. Hu, J. Jin, Y. Yin, H. Zhang, C. Cai, Direct electrochemistry of glucose oxidase assembled on graphene and application to glucose detection, Electrochim. Acta 55 (2010) 8606–8614.
[75] R. Garjonyte, Y. Yigzaw, R. Meskys, A. Malinauskas, L. Gorton, Prussian Blue- and lactate oxidase-based amperometric biosensor for lactic acid, Sens. Actuators B Chem. 79 (2001) 33–38.
[76] A. Sannini, D. Albanese, F. Malvano, A. Crescitelli, M. Di Matteo, An amperometric biosensor for the determination of lactic acid during malolactic fermentation, Chem. Eng. Trans. 44 (2015) 283–288.
[77] A. Caliò, P. Dardano, V. Di Palma, M.F. Bevilacqua, A. Di Matteo, H. Iuele, L. De Stefano, Polymeric microneedles based enzymatic electrodes for electrochemical biosensing of glucose and lactic acid, Sens. Actuators B Chem. 236 (2016) 343–349.
[78] M.M.F. Choi, Application of a long shelf-life biosensor for the analysis of L-lactate in dairy products and serum samples, Food Chem. 92 (2005) 575–581.
[79] Y.M. Choi, H. Lim, H.N. Lee, Y.M. Park, J.S. Park, H.J. Kim, Selective nonenzymatic amperometric detection of lactic acid in human sweat utilizing a multi-walled carbon nanotube (MWCNT)-polypyrrole core-shell nanowire, Biosensors 10 (2020) 111.
[80] M. Yang, J. Wang, H. Li, J.G. Zheng, N.N. Wu, A lactate electrochemical biosensor with a titanate nanotube as direct electron transfer promoter, Nanotechnology 19 (2008) 075502.
[81] T. Xia, G. Liu, J. Wang, S. Hou, S. Hou, MXene-based enzymatic sensor for highly sensitive and selective detection of cholesterol, Biosens. Bioelectron. 183 (2021) 113243.
[82] N. Ruecha, W. Siangproh, O. Chailapakul, A fast and highly sensitive detection of cholesterol using polymer microfluidic devices and amperometric system, Talanta 84 (2011) 1323–1328.
[83] C. Hong, X. Zhang, C. Wu, Q. Chen, H. Yang, D. Yang, Z. Huang, R. Cai, W. Tan, On-site colorimetric detection of cholesterol based on polypyrrole nanoparticles, ACS Appl. Mater. Interfaces 12 (2020) 54426–54432.
[84] M. Thiruppathi, C.Y. Tsai, T.W. Wang, Y. Tsao, T.H. Wu, Simple and cost-effective enzymatic detection of cholesterol using flow injection analysis, Anal. Sci. 36 (2020) 1119–1124.
[85] M.K. Ram, P. Bertoncello, H. Ding, S. Paddeu, C. Nicolini, Cholesterol biosensors prepared by layer-by-layer technique, Biosens. Bioelectron. 16 (2001) 849–856.
[86] U. Saxena, M. Chakraborty, P. Goswami, Covalent immobilization of cholesterol oxidase on self-assembled gold nanoparticles for highly sensitive amperometric detection of cholesterol in real samples, Biosens. Bioelectron. 26 (2011) 3037–3043.
[87] S. Wang, S. Chen, K. Shang, X. Gao, X. Wang, Sensitive electrochemical detection of cholesterol using a portable paper sensor based on the synergistic effect of cholesterol oxidase and nanoporous gold, Int. J. Biol. Macromol. 189 (2021) 356–362.
[88] M.J. Cooney, Kinetic measurements for enzyme immobilization, Methods Mol. Biol. 1504 (2017) 215–232.
[89] D. Lan, B. Li, Z. Zhang, Chemiluminescence flow biosensor for glucose based on gold nanoparticle-enhanced activities of glucose oxidase and horseradish peroxidase, Biosens. Bioelectron. 24 (2008) 934–938.
[90] S. Garcia-Rey, E. Ojeda, U.B. Gunatilake, L. Basabe-Desmonts, F. Benito-Lopez, Alginate bead biosystem for the determination of lactate in sweat using image analysis, Biosensors 11 (2021) 379.